Debashis Pal[1]
Suman Chakraborty[2]

[1]Advanced Technology Development Centre, IIT Kharagpur, Kharagpur, India
[2]Mechanical Engineering Department, IIT Kharagpur, Kharagpur, India

Received June 5, 2010
Revised October 12, 2010
Accepted October 23, 2010

Research Article

An analytical approach to the effect of finite-sized end reservoirs on electroosmotic transport through narrow confinements

The presence of end reservoirs often alters the electrical potential distributions inside narrow fluidic confinements of electrokinetically actuated miniaturized devices to a significant extent. This paper examines the influence of finite size effect of the end reservoirs on the concerned potential distribution analytically, using the Schwarz–Christoffel conformal mapping. The effective electric field directly acting across the channel is accordingly represented by a calibration curve, which sums up the role of the key geometric parameters (reservoir-to-channel height and length ratios) on the potential distribution. The analytical model is further augmented to assess the flow characteristics through the channel. The results indicate that the alterations in the flow characteristics due to alterations in the effective electric field on account of the finite size effects of the end reservoirs can turn out to be significantly more prominent than the corresponding alterations due to the axial pressure gradients induced by the sudden contraction and expansion effects associated with the end reservoirs. The derived results can be further utilized to facilitate the practical design of miniaturized fluidic devices, using conveniently tractable analytical tools.

Keywords:
Electroosmotic transport / End reservoir effect / Schwarz–Christoffel mapping
DOI 10.1002/elps.201000308

1 Introduction

Precise flow control often turns out to be critical toward realizing the desired transport characteristics in electrosmotically actuated miniaturized fluidic devices [1–4]. It is well known that in contact with an electrolyte solution, several microfluidic substrates (such as glass, PDMS) tend to acquire a net electrical charge. As a result, the nearby counter-ions in the solution are attracted toward the surface, while co-ions are repelled. At equilibrium, a balance between the electrostatic interactions and thermal agitation generates a charge density profile in the solution. Thus, a counter-ion concentration gradient establishes within the liquid, with a higher concentration near the solid surface and a lower concentration in the far-stream. This counter-ion-rich region near the wall is called the electric-double-layer (EDL) [5] and the associated electric potential is known as induced potential (ψ). When a straight channel is exposed to an axially acting external electric field, the counter-ions in the EDL move under the action of electrostatic forces. Due to a cohesive nature of the hydrogen bonding in the polar solvent molecules, the entire buffer solution is pulled, leading to a net electrokinetic body force on the bulk fluid, which is a combined function of the local charge density gradients and the imposed electrical field. Electrically neutral liquid, far away from the solid wall, is also set into motion through viscous drag, thereby actuating a fluid flow in the entire domain.

The physical arrangement of generating electroosmotic flows, in practice, may get substantially more involved than that depicted by the standard description based on the mere presence of a straight channel. Such additional complexities may stem from the fact that to generate the electrokinetic force, the channel is connected to two reservoirs (inflow and outflow) at the upstream and the downstream ends, in which the actuating electrodes are submerged. Once as a certain electrical-potential difference is applied between the two electrodes, an electric field is generated within the channel. The distribution of electric field within the channel, in effect, depends on the shape and size of the end reservoirs. The applied potential difference between the electrodes, in reality, may be significantly different from the effective potential difference prevailing between the

Correspondence: Dr. Suman Chakraborty, Mechanical Engineering Department, IIT Kharagpur, Kharagpur 721302, India
E-mail: suman@mech.iitkgp.ernet.in
Fax: +91-3222-282278

Abbreviation: SCM, Schwarz–Christoffel conformal mapping

entrance and exit of the channel. Ignoring the effect of the end reservoirs on the potential distribution, thus, may incur serious errors in the solution of electroosmotic flow. Moreover, reservoirs can also affect the system performance by generating an additional adverse pressure gradient in the flow direction.

Traditionally, in electroosmotic flow literature, the external electric field driving the flow is often ascertained by dividing the applied potential difference by the length between the electrodes without considering the details of the reservoir design. In reality, however, the electrodes may be placed at one side of the respective reservoirs and away from the channel entrance/exit. As a result, the electrical potentials at the channel ends are not the same as those ones of the corresponding electrodes. Therefore, the actual potential distribution within the channel may differ significantly from the distribution calculated from traditional considerations. To the best of the knowledge of the authors, there have been very few studies on the effect of the end reservoirs and the electrodes contained in the same on the electrical field distribution and the consequent flow solution. Although the effect of embedded electrodes in microchannels has been analytically studied by previous researchers [6], effects of reservoirs have not been considered in those investigations. In another study by Suh et al. [7], two separate analytical solutions – one for the reservoir and the other for the channel region – have been obtained for the potential distribution, and then a numerical solution has been employed to patch those in order to obtain the complete electric field. However, these solutions [7] are limited by the fact that these are asymptotically correct for vanishingly small electrode sizes and limitingly small channel heights only. An additional complication of the presence of reservoirs in the fluidic systems is the introduction of axial pressure gradient due to sudden contraction and expansion at channel entrance and exit. Such abrupt change in cross-sectional area is likely to cause significant viscous dissipation which in turn leads to the irreversible pressure losses at both inlet and exit sections of the channel. Since both the reservoirs are kept at same pressure, electroosmotic flow has to adjust to those pressure boundary conditions by inducing an adverse pressure gradient along the stream-wise direction [8–10]. It is important to recognize here that the electroosmotic driving mechanism actually needs to overcome this adverse pressure field in order to maintain unidirectional fluidic transport. Additionally, the induced pressure gradients might cause band broadening effects [11, 12], which could be detrimental to the performance of fluidics-based separation systems. Therefore, theoretical models for electroosmotically driven flows must take into account the effects of induced pressure fields, so as to design fluidic systems consistent with practically realizable conditions. The induced pressure field, in turn, may have an interesting coupling with the electroosmotic mechanisms, bearing significant consequences on the overall transport [13, 14].

In this paper we evaluate the electric field in a channel connected to end reservoirs using an analytical technique, called the Schwarz–Christoffel conformal mapping (SCM). Unlike the work by Suh et al. [7], a single solution for the potential distribution is prescribed for the entire domain without imposing any restrictions on the electrode size or channel height. The analytical results are validated by solving the Laplace equation numerically using a finite volume method. To estimate the effect of reservoir size on the potential distribution, critical geometric parameters such as the ratio of reservoir height to channel height (H/h) and the ratio of channel length to total length (L_C/L) are identified. The effective potential difference between the entrance and exit of the channel is plotted as a function of L_C/L and H/h, which may form a fundamental design basis for electroosmotically driven fluidic systems. In order to investigate the effect of reservoir on the flow solution, a generalized analytical model is accordingly developed, on the basis of the effective potential from equivalent straight channel considerations. The EDL potential field is obtained using the full Poisson–Boltzmann equation [5], instead of going through the routes of the commonly presumed Debye–Hückel linearization. The routinely neglected pressure losses at the inlet and exit sections of the channel are aptly taken into account, in order to accurately describe the flow physics. To validate the analytical solution, full-scale numerical simulation studies are also performed, considering the detailed flow features with explicit accounting of the end reservoirs. Numerically, the concentration fields of ions and the induced potential (ψ) distribution are obtained by solving the ion conservation equation (the Nernst–Planck equation) and the Poisson equation, respectively.

2 Problem formulation and analysis

2.1 Analytical solution for the externally applied electric field

In order to obtain the distribution of external electric potential (ϕ), we consider a geometry composed of a channel connected to identical rectangular reservoirs at both ends, as shown in Fig. 1. Important dimensions are channel length (L_C), length of the reservoir (L_R), channel height (h) and height of the reservoir (which is taken to be the same as the width of the electrodes, H). Typically, the wall surfaces have a much smaller permittivity and conductivity than the electrolyte in the channel; therefore,

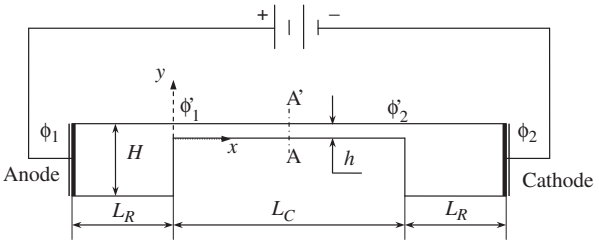

Figure 1. A fluidic channel connecting two identical reservoirs.

we assume all the surrounding boundaries except the electrode surface to be perfectly insulated (no leakage in electric field). The electric potentials at anode and cathode are ϕ_1 and ϕ_2, respectively. The effective potential difference between the entrance and exit of the channel is $\Delta\phi_{channel} = (\phi_1' - \phi_2')$. Since the electrodes are long compared to their width, the problem reduces to two dimensions, allowing the SCM method to be applicable.

Exploiting the symmetry of the problem, we consider only one half of the entire domain, as shown in Fig. 2(A). The geometry is defined in the complex z-plane, with coordinates $z = x+iy$. The left boundary (referring to the dashed-dotted line AA′ in Fig. 1) represents the mid-section of the microchannel, and the potential at this section ϕ_a is simply the average of ϕ_1 and ϕ_2. The cathode is replaced by the boundary DD′, which is defined by the points $\mathrm{Real}(z) = L_R$. All other boundaries representing channel or reservoir walls assume zero-flux condition, i.e. $\partial\phi/\partial n = 0$, where n is the normal to the boundary. The x–y axes shown in Fig. 2(A) are so chosen to facilitate the mapping only; for flow solution the axes are translated to the entrance of channel as shown in Fig. 1.

The problem now consists of transforming the interior of the polygon A′ABCDD′ into the upper half of the τ-plane ($= \xi+i\eta$) so that the boundaries AA′, AB, BC, etc. are all mapped onto the real axis ($\eta = 0$) of τ-plane. This task is accomplished by the SCM technique [15, 16]. The corresponding Schwarz–Christoffel integral from the τ-plane to the z-plane is given by

$$z = f(\tau) = \frac{1}{K}\int \sqrt{\frac{\tau-b}{\tau-c}}\frac{d\tau}{(\tau-a)} + C_0 \quad (1)$$

where a, b, c, etc. are the points on the real axis of the τ-plane corresponding to the vertices A, B, C, etc. The constant K determines the scale of the polygon and its orientation, while the constant of integration C_0 determines the location of the origin in the physical z-plane. Of the constants a, b, c, d, etc. any three may be chosen arbitrarily (typically 0, 1, ∞) and any remaining ones will be determined by the shape of the polygon [17]. In this problem, points A and A′ shrink to the origin ($\tau = a = 0$); whereas points D and D′ are respectively mapped to positive infinity and negative infinity of τ-plane. Constant b is chosen as 1, whereas the constant c is to be determined. Therefore, three conditions for the points A, B, and C are:

Tranformed τ−plane	Physical z−plane
$\tau = a = 0$	$\mathrm{Real}(z) \to -\infty$
$\tau = b = 1$	$z = B = i(H-h)$
$\tau = c$	$z = C = 0$

Integrating (1) and applying the above stated conditions, we obtain

$$c = (H/h)^2$$

and

$$z = f(\tau) = \frac{H}{\pi}\left[\ln\left(\frac{1+s}{1-s}\right) - \frac{h}{H}\ln\left(\frac{H/h+s}{H/h-s}\right)\right] \quad (2)$$

where $s = \sqrt{\frac{\tau-c}{\tau-b}} = \sqrt{\frac{\tau-(H/h)^2}{\tau-1}}$. The function $f(\tau)$ is analytic. With a two-dimensional point charge (source or sink) located at the origin of τ-plane, the solution for the electric field in the physical z-plane is given by the complex potential

$$W \equiv \phi(x,y) + i\,\varphi(x,y) = m\ln(\tau) \quad (3)$$

where m is the strength of the source or sink. Noting that any complex number can be expressed in a polar form $re^{i\theta}$, the distribution of electric field potential inside the channel as well as reservoir turns out to be

$$\phi(x,y) = m\ln(r) + c_0 \quad (4)$$

where c_0 is a constant added to accommodate the boundary condition on ϕ, and it does not affect the electric field.

To sum up, any point with a radial coordinate r in the τ-plane can be mapped into a point (x, y) in the z-plane and the electric potential at that point is given by Eq. (4). The procedure of determining z and its corresponding potential ϕ for given values of L_C, L_R, h, and H is briefly described in the Supporting Information (Appendix).

Potential distribution in the other half of the domain (anode side) can be obtained using symmetry considerations. Once the potential distribution, $\phi(x, y)$, is obtained for the entire domain, the external electric field is derived as: $E_{ext}(x, y) = -\nabla\phi$.

2.2 Governing equations and numerical formulation

Fundamentally, electroosmotic flow is actuated by the interactions of ions in the EDL with an externally imposed electric field (E_{ext}). According to the laws of electrostatics, the externally applied electric potential (ϕ) obeys the Laplace equation

$$\nabla^2\phi = 0 \quad (5)$$

which, in the present case, is subjected to the insulating boundary conditions on all the surfaces except the electrodes.

The induced electrokinetic potential (ψ) due to the wall surface charging is related to the net charge density, ρ_e, through the Poisson equation

$$\nabla^2\psi = -\frac{\rho_e}{\varepsilon} \quad (6)$$

where ε is the electrical permittivity of the solution. For a symmetric electrolyte (co-ions and counter-ions have equal charge valence, i.e. $z^+ = -z^- = z$), the local charge density per unit volume, ρ_e, is given by,

$$\rho_e = ze(n^+ - n^-) \quad (7)$$

Here n^+ and n^- represent ionic number concentrations of positive and negative charges, respectively, and e is the elementary protonic charge. Regarding the boundary condition on induced potential (ψ), we assume $\psi = \zeta$ (constant zeta potential) at the channel walls and $\psi = 0$ at the other solid boundaries. Further, at the inlet and outlet of the domain $\partial\psi/\partial x = 0$.

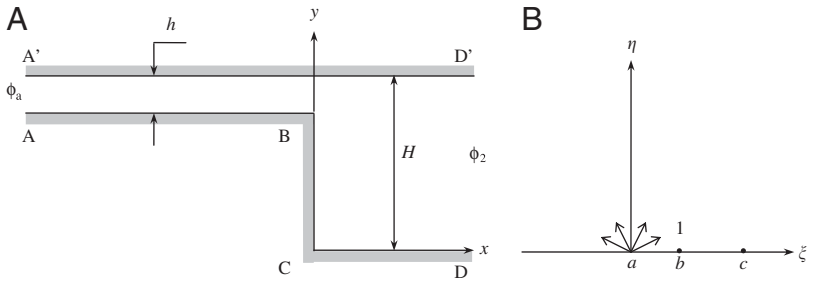

Figure 2. (A) Physical *z*-plane, composed of half of the channel and reservoir at one side, and (B) the transformed τ-plane with a source of electric field at origin.

Formally, the modeling of a reservoir-channel system, as depicted in Fig. 1, involves transport of the ionic species. Accordingly, the ionic concentration field (n^+ and n^-) is obtained by employing the ionic species conservation equation (the Nernst–Planck equation [18])

$$\frac{\partial n^{\pm}}{\partial t} + \vec{V} \cdot \nabla n^{\pm} = \nu z F \, \nabla.(n^{\pm} \nabla(\phi + \psi)) + D\nabla^2 n^{\pm} \tag{8}$$

where $\vec{V}$ is the flow velocity field, F is the Faraday constant, ν and D are mobility and diffusion coefficient of the ions, respectively. The parameters D and ν are (both assumed to be equal and constants for anions and cations) related by the Stokes–Einstein relationship, $D = \nu RT$, where R is universal gas constant and T is the absolute temperature. Equation (8) is specially required near the reservoir channel junction where equilibrium Boltzmann distributions of ions [5] are not valid owing to the abrupt changes in local electric fields and the flow geometry. Another advantage of using the Nernst–Planck equation is that the consideration of convention effect on ionic distribution makes the present study a foolproof one. Equation (8) is subjected to the following boundary conditions: at the inlet $n^+ = n^- = n_0$, at the outlet $\partial n^+/\partial x = \partial n^-/\partial x = 0$, and at the walls, local thermodynamic equilibrium prevails such that $n^-|_{\text{wall}} = n_0 e^{ze\zeta/k} B^{\text{T}}$ and $n^+|_{\text{wall}} = n_0 e^{-ze\zeta/k} B^{\text{T}}$ based on the Boltzmann distribution [5]. Here, n_0 is the average number of positive or negative ions in the buffer, k_{B} is the Boltzmann constant, and $\zeta = 0$ at the reservoir walls. The ionic number densities, n^+ and n^-, obtained by solving Eq. (8) give us the local charge density through Eq. (7), which is substituted in the Poisson equation (Eq. 6) to obtain the distribution of EDL potential (ψ).

The flow field is governed by the coupled continuity and momentum conservation equations, described as follows:

$$\nabla \cdot \vec{V} = 0 \tag{9}$$

$$\frac{\partial}{\partial t}(\rho \vec{V}) + \nabla \cdot (\rho \vec{V}\vec{V}) = -\nabla p + \nabla \cdot (\mu \nabla \vec{V}) + \rho_e \vec{E} \tag{10}$$

where ρ is the fluid density, p is the pressure, μ is the fluid viscosity and $\vec{E}$ is the resultant electric field (a combined consequence of the applied and the induced EDL potential, i.e. $\vec{E} = -\nabla(\phi + \psi)$).

Equations (5), (6) and (8–10) are simultaneously solved in a two-dimensional framework by employing a fully time implicit finite volume technique, leading to a steady-state solution of the velocity field. A coupling between the pressure and velocity is accomplished by using the SIMPLE algorithm [19]. A variable size grid system is considered and a smooth spatial variation in the grid-size is maintained, with more densely spaced grids being skewed close to the solid boundaries. The discretized system of linear algebraic equations is numerically solved by employing the line-by-line tridiagonal matrix algorithm (TDMA). Convergence criterion for the maximum relative errors in all the discretized equations is set to 10^{-6}.

2.3 Simplified analytical model

In order to gain a deeper physical insight into the physical system under consideration, approximate analytical solutions corresponding to certain simplified considerations are also obtained. It is assumed that the system is in electrochemical equilibrium and the fluid flow does not influence the ionic concentration distributions (and hence the electrical potential). Thus, n^+ and n^- can be described by the equilibrium Boltzmann distribution [5]: $n^- = n_0 e^{ze\psi/k} B^{\text{T}}$ and $n^+ = \psi e^{-ze\psi/k} B^{\text{T}}$. With these considerations, Eqs (6) and (7) can be combined together to obtain the following governing equation for the EDL potential (ψ):

$$\nabla^2 \psi = \frac{2 n_0 z e}{\varepsilon} \sinh\left(\frac{ze\psi}{k_{\text{B}} T}\right) \tag{11}$$

which is nothing but the well-known Poisson–Boltzmann equation. The variables appearing in the above equations can be non-dimensionalized by employing suitable non-dimensional parameters such as $\bar{x}_j = 2x_j/h$ and $\bar{\psi} = ze\psi/k_B T$, so as to obtain

$$\nabla^2 \bar{\psi} = k^2 \sinh(\bar{\psi}) \tag{11a}$$

where $k = \kappa h/2$, with $\kappa = 1/\lambda_{\text{D}} = (2n_0 z^2 e^2/\varepsilon k_B T)^{1/2}$. Here, κ is the Debye–Hückel parameter. Reciprocal of κ is called characteristic thickness (λ_{D}) of the EDL, which can vary from a few nanometers to even a micrometer, depending on the concentration of the electrolyte (the higher the ion concentration, the lower the EDL thickness). The coefficient k in Eq. (11a) is referred to as the double-layer thickness parameter [9]. The average number of positive or negative ions in the buffer n_0 is given by, $n_0 = 1000 C N_{\text{A}}$, where C is the molar concentration of ions, N_{A} is Avogadro's number. As a next step, an equivalent one-dimensional form of Eq. (11) is analytically solved. Undoubtedly, the simplifications originating from an

equivalent one-dimensional formulation tend to disturb the accuracy of the solution of the local field variables to some extent (although we demonstrate later on that such discrepancies are negligible so far as the flow field within the channel is concerned, provided appropriate physical considerations are aptly taken into account). It is observed that the equilibrium Boltzmann distributions of charges remain unperturbed by the flow field and/or applied voltages only when both the applied electric field (E_{ext}) and the velocity field are everywhere tangent to the surfaces of equal equilibrium charge densities [20, 21]. In a channel–reservoir system, as shown in Fig. 1, these conditions are satisfied in the interior of a channel (which is sufficiently long) with uniform wall surface charge. However, near the channel reservoir junction Boltzmann distributions are not applicable owing to the local surface charge discontinuities and abrupt changes in flow geometry. Moreover, the Poisson–-Boltzmann equation predicts absurdly high ion concentrations when the surface potential is large [22, 23], because it neglects the ion–ion interactions and steric effects. Irrespective of such limitations, we intend to compare the analytically predicted flow fields with those obtained from the full-scale numerical simulations based on the Nernst–-Planck equation, which stands for a more general approach. It is important to mention in this context that our important endeavor is also to assess the predictive capability of the analytical model in terms of flow rates, which happens to be one of the critical system design considerations. With such objectives in view, the following boundary conditions: $\psi = \zeta$ at $y = 0,\ h$; $\psi \to 0$ at channel center line ($y = h/2$), can be collectively employed to obtain the resultant induced potential distribution from the Poisson–Bolzmann equation-based analytical model (using Eqs. 11), as

$$\psi(y) = \zeta\left[\left(\frac{4}{\alpha}\right)\tanh^{-1}\left\{\tanh\left(\frac{\alpha}{4}\right)\exp(-\kappa y)\right\}\right] \tag{12}$$

where y is the distance measured from the channel wall, $\kappa = 1/\lambda_D$ is the Debye–Hückel parameter, and $\alpha = ze\zeta/k_BT$ is the ionic energy parameter. The above closed-form solution, in terms of an explicit function of the coordinate y, is obtained without invoking the Debye–Hückel linearization principle [2, 5], and hence it is valid even for high value of surface potential ($|\zeta| > 25$ mV). It can be noted that unlike Debye–Hückel linearized solution, distribution of ψ in Eq. (12) is an explicit function of the ionic energy parameter, α.

An approximate analytical solution for the velocity field can be obtained by neglecting the transverse velocity component as compared with that of the axial one ($u >> v$), and by neglecting the axial diffusion term as compared to the corresponding transverse diffusion term, so that one gets

$$\mu\frac{\partial^2 u}{\partial y^2} - \rho_e\frac{\partial(\phi+\psi)}{\partial x} = \frac{\partial p}{\partial x} \tag{13}$$

and

$$-\rho_e\frac{\partial(\phi+\psi)}{\partial y} = \frac{\partial p}{\partial y} \tag{14}$$

Since the left-hand sides of Eqs. (13) and (14) are functions of y only, the pressure field needs to satisfy the following constraints:

$$\frac{\partial}{\partial x}\left[\frac{\partial p}{\partial x}\right] = 0 \quad \text{and} \quad \frac{\partial}{\partial x}\left[\frac{\partial p}{\partial y}\right] = 0$$

Thus, one may express the pressure field p in the following form:

$$p(x, y) = C_1 x + C_2 + f(y) \tag{15}$$

where C_1 and C_2 are constants. Substituting Eq. (15) into Eq. (13), one gets

$$-C_1 + \mu\frac{\partial^2 u}{\partial y^2} - \rho_e\frac{\partial\phi}{\partial x} = 0 \tag{16}$$

Using Eq. (6) for ρ_e, we obtain

$$-C_1 + \mu\frac{\partial^2 u}{\partial y^2} + \varepsilon\left(\frac{\partial\phi}{\partial x}\right)\frac{\partial^2\psi}{\partial y^2} = 0 \tag{17}$$

This equation is linear, and hence we can decompose the velocity field into two parts [14]

$$u = u_{PDF} + u_{EOF}$$

where u_{PDF} is the pressure driven flow velocity in a 2D channel (i.e. plane Poiseuille flow) and u_{EOF} corresponds to the velocity of pure electroosmotic flow. In the absence of axial pressure gradient, we can assume $C_1 = 0$. However, irreversible viscous pressure losses occur at the channel inlet and outlet because of sudden flow contraction and expansion. This leads to an adverse axial pressure gradient inside the channel even when we maintain same pressure (P_0) at both the reservoirs. Employing no-slip wall boundary conditions and using superposition principle for linear equations, we obtain the following velocity profile:

$$u = -\frac{C_1 h^2}{2\mu}\left[\frac{y}{h} - \left(\frac{y}{h}\right)^2\right] + \frac{\varepsilon\zeta}{\mu}\left(\frac{\partial\phi}{\partial x}\right)\left[1 - \frac{\psi}{\zeta}\right] \tag{18}$$

Employing the solution for (Eq. 12), this velocity profile can be integrated to obtain the volume flow rate per unit width ($w = 1$) of the channel

$$Q = -\frac{C_1 h^3}{12\mu} + U_{HS}h[1 - q] \tag{19}$$

where, $U_{HS} = \frac{\varepsilon\zeta}{\mu}\left(\frac{\partial\phi}{\partial x}\right)$ is Helmholtz–Smoluchowski electroosmotic velocity, $E_{eff} = -\frac{\partial\phi}{\partial x}$ is the effective electric field acting across the channel, and

$$q = \frac{4}{\alpha}\left[\tanh^{-1}\left(\frac{1}{B}\right) - \frac{1}{2}\{\ln(1+B) - \ln(1-B)\}\right.$$
$$\left. - \frac{1}{2k}\{\mathrm{Li}_2(-B) - \mathrm{Li}_2(B) - \mathrm{Li}_2(-B_o) + \mathrm{Li}_2(B_o)\}\right] \tag{20}$$

$$\text{with} \quad \frac{1}{B} = \tanh(\alpha/4)\exp(-k), \quad \frac{1}{B_o} = \tanh(\alpha/4)$$

Here, $\mathrm{Li}_2(B)$ is dilogarithm, a special function defined by the integral [24, 25],

$$\mathrm{Li}_2(B) = -\int_0^B \frac{\ln(1-t)}{t}\,dt \tag{20a}$$

The above definition is valid for arbitrary B. In case of $B \geq 1$ the integral expression for the dilogarithm can be written as

$$\mathrm{Li}_2(B) = \frac{\pi^2}{6} - \int_1^B \frac{\ln(1-t)}{t}\,\mathrm{d}t - \mathrm{i}\pi\ln(B) \tag{20b}$$

from which expanding $\ln(t-1)$ and integrating term by term we obtain

$$\mathrm{Li}_2(B) = \frac{\pi^2}{3} - \frac{1}{2}(\ln(B))^2 - \sum_{k=1}^{\infty}\frac{1}{k^2 B^k} - \mathrm{i}\pi\ln(B) \tag{20c}$$

For $|B| < 1$, dilogarithm can be evaluated as the sum

$$\mathrm{Li}_2(B) = \sum_{k=1}^{\infty}\frac{B^k}{k^2} \tag{20d}$$

The parameter q depends only on the double-layer thickness parameter (k) and ionic energy parameter (α). It is evident that for a given value of α (say, 4), as $k \to \infty$, the first term in q tends to zero, and the second term $\to -\mathrm{i}\pi/2$. Moreover, there is no restriction on the value of α; accordingly, a high magnitude of the zeta potential (ζ) is acceptable for Eq. (18), unlike the Debye–Hückel linearized solution which is valid for $|\zeta| \leq 25$ mV.

It is important to mention here that an accurate estimation of the net flow rate through the channel heavily depends on a consistent estimation of $E_{\mathrm{eff}} = -\frac{\partial\phi}{\partial x}$. Interestingly, when a channel is connected to inflow and outflow reservoirs equipped with the electrodes (refer to Fig. 1), the effective electric field within the channel (E_{eff}), as predicted by the SCM, will be different from the average electric field (E_{avg}), where effective and average fields are given by,

$$E_{\mathrm{eff}} = (\phi_1' - \phi_2')/L_{\mathrm{C}} \tag{21a}$$

$$E_{\mathrm{avg}} = (\phi_1 - \phi_2)/(L_{\mathrm{C}} + 2L_{\mathrm{R}}) \tag{21b}$$

Equation (19) confirms trivially that in the absence of axial pressure gradient ($C_1 = 0$), the ratio of volume flow rates due to the actual electric field and the approximate (averaged) electric field is simply the ratio of these two fields and independent of any other parameter including k. However, in the presence of any axial pressure gradient, such a comment cannot be trivially made and further analysis may be necessary. Toward that, it is important to recognize that Eq. (19) contains an undetermined parameter C_1, which is an effective indicator of the axial pressure gradient, and may need to be judiciously obtained. This aspect is elucidated in the foregoing paragraph.

The average velocity can be obtained from Eq. (19) in a straightforward manner, as

$$u_{\mathrm{avg}} = -\frac{C_1 h^2}{12\mu} + U_{\mathrm{HS}}[1-q] \tag{22}$$

The undetermined parameter C_1 needs to be determined from the considerations of the flow-induced pressure drops at the inlet and the exit sections of the channel, mentioned as earlier. Considering the channel to be long enough such that the flow development length is smaller in comparison to the total length of the channel (L_{C}), the fluid pressure at the inlet section can be determined as [8]

$$p_{\mathrm{in}} = P_0 - \Delta P_{\mathrm{in}} \tag{23}$$

where $\Delta P_{\mathrm{in}} = \frac{1}{2}\rho\bar{u}_{\mathrm{in}}^2 + \delta p_{\mathrm{in}}$. Here $\bar{u}_{\mathrm{in}}$ is the mean inlet velocity, δp_{in} is the pressure loss at the entrance and P_0 is the atmospheric pressure, which is same as reservoir pressure. The term $\frac{1}{2}\rho\bar{u}_{\mathrm{in}}^2$ in the expression for ΔP_{in} can be neglected for creeping flows. For creeping flow through an infinitely thin slit, the integrated pressure loss due to flow contraction and expansion can be evaluated from the theory developed by Roscoe [26], as

$$\delta p_{\mathrm{total}} = \frac{32}{\pi}\frac{\mu u_{\mathrm{avg}}}{h} \tag{24}$$

where u_{avg} is the average flow velocity as a combined consequence of the electroosmotic and the pressure field. With pressure losses at the inlet and the exit sections being virtually identical for creeping flows, one may write $\Delta P_{\mathrm{in}} \simeq \delta p_{\mathrm{in}} = 0.5\delta p_{\mathrm{total}} = (16/\pi)(\mu/h)u_{\mathrm{avg}}$. From analogous considerations, one may also determine the exit pressure as [8]

$$p_{\mathrm{out}} = P_0 + \Delta P_{\mathrm{out}} \tag{25}$$

where $\Delta P_{\mathrm{out}} = (16/\pi)(\mu/h)u_{\mathrm{avg}}$.

Noting that the average pressure gradient can be estimated as $\delta p_{\mathrm{total}}/L_{\mathrm{C}}$, one can utilize Eqs. (22) and (24) to obtain

$$C_1 = \frac{32}{\pi}\frac{\mu}{hL_{\mathrm{C}}}\left[-\frac{C_1 h^2}{12\mu} + U_{\mathrm{HS}}(1-q)\right] \tag{26}$$

On solving for C_1 from Eq. (26), one gets

$$C_1 = \frac{96\mu U_{\mathrm{HS}}(1-q)}{3\pi h L_{\mathrm{C}} + 8h^2} \tag{27}$$

Equation (27) leads to an approximate description of the axial the velocity profile in the following form:

$$u = U_{\mathrm{HS}}\left[1 - \frac{4}{\alpha}\tanh^{-1}\left\{\tanh\left(\frac{\alpha}{4}\right)\exp\left(-\frac{k\gamma}{h/2}\right)\right\} - \frac{48(1-q)}{3\pi(L_{\mathrm{C}}/h)+8}\left\{\frac{\gamma}{h} - \left(\frac{\gamma}{h}\right)^2\right\}\right] \tag{28}$$

From this equation it is evident that the pressure gradient effect decreases with the increased channel aspect ratio (L_{C}/h), which is in agreement with the observations of Zhang et al. [8]. Since the reference velocity (U_{HS}) is common to every term in the right-hand side of this equation, we expect the flow rate ratio with the effective and the average electrical fields to be dictated solely by the ratio of the respective electric fields even in the presence of axial pressure gradient induced by sudden expansion and contraction, provided all other relevant parameters remain same. This can be verified numerically by solving the entire set of governing equations (Eqs. 5, 6 and 8–10) and considering full system geometry including the reservoirs.

3 Results and discussions

3.1 Assessment of the SCM (analytical) method

In order to validate the conformal mapping technique (SCM), we solve Eq. (5) numerically using a fully implicit finite volume formulation [19] with a Neumann boundary condition ($\partial\phi/\partial n = 0$) at all solid the boundaries except at the electrode ($\phi = -50$ V). These voltages are measured relative to the potential at the channel mid-section (i.e. left end of the domain depicted in Fig. 3). The potential distributions (ϕ) due to the applied electric field, as predicted by the SCM and the finite volume method, are compared in Fig. 3. Reasonably good agreements are obtained between the solutions obtained from these two methods, as evident from the figure.

3.2 Effective potential difference across the channel: Dependence on L_C/L and H/h

Using the analytical technique described above, we obtain a set of ''design curves'' that readily give us the effective potential difference between the entrance and exit of the channel ($\Delta\phi_{channel}$) from the potential difference between the electrodes ($\Delta\phi_{electrode}$). The ratio of these two quantities, called Voltage Ratio, is plotted as a function L_C/L for various H/h; where L is the distance between the electrodes ($= L_C + 2L_R$), as depicted in Fig. 4, for a few representative cases. The average axial electric field between the electrodes is given by $E_{avg} = \Delta\phi_{electrode}/(L_C+2L_R)$. For a given $\Delta\phi_{electrode}$, the curves depicted in Fig. 4 give us an equivalent axial electric field ($E_{eff} = \Delta\phi_{channel}/L_C$) that can be directly fed into a simple one-dimensional analysis to obtain the correct flow solution within the channel, without going for an expensive two-dimensional simulation. These curves, therefore, form an important design basis for one-dimensional electroosmotic flow analysis, since they account for the effect of the change in ϕ due to the reservoirs. As H/h increases, these characteristic curves tend to flatten and get parallel to the horizontal axis, implicating a less emphatic dependence of the voltage ratio on the H/h ratio. In the limit of channel-without-reservoir, $H \to h$, so that the characteristic curve becomes a straight line joining (0, 0) and (1, 1). In the limit of a very long channel ($L_C/L \to 1$), the voltage ratio $\to 1$. On the other hand, in the limit of an axially very short channel ($L_C/L \to 0$), the voltage ratio drops to 0. It is important to mention in this context that the curves depicted in Fig. 4 are by no means exhaustive, and are mere illustrations of the predictive capabilities of the analytical model in terms of ascertaining the effective electric field across the channel from the information of the imposed electric field, based on other chosen design conditions. One may construct several such similar characteristics with various other channel aspect ratios (L_C/h) and reservoir to channel height ratios (H/h), which we omit here for the sake of brevity.

It is also important to mention here that the velocity profiles derived analytically in this work (by using $\Delta\Phi_{channel}$ from the calibration curve) are compared with the velocity profiles obtained through detailed numerical simulations. Such comparisons, however, are not reproduced here for the sake of brevity. Please see the Supporting Information for the pertinent details.

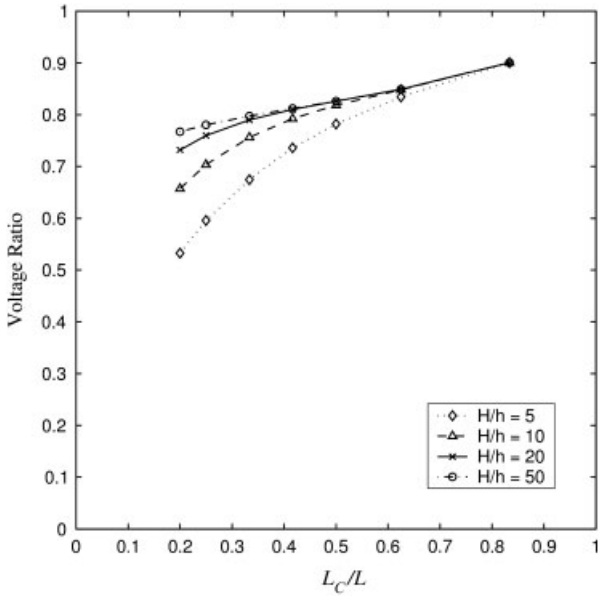

Figure 4. Voltage ratio ($\Delta\phi_{channel}/\Delta\phi_{electrode}$) for a given channel with $L_C/h = 20$.

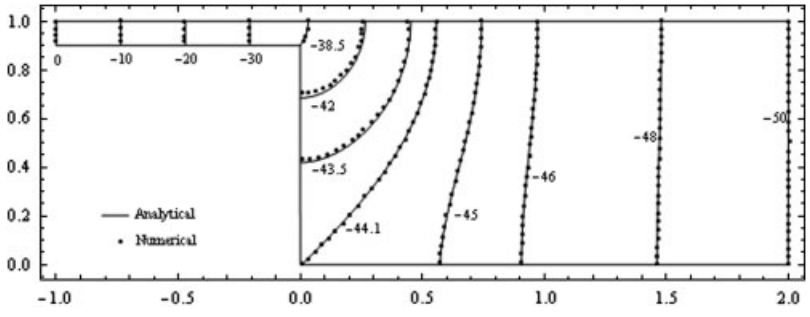

Figure 3. Potential distribution (ϕ) due to the applied electric field inside the half-channel and outflow reservoir. The numerical solution is presented by dots, whereas solid lines represent the analytical solutions.

4 Concluding remarks

Reservoirs are indispensable in microfludic devices. The presence of finite-sized reservoirs at the ends of a microchannel can influence the system performance in two ways – first, they alter the external electric field within the channel and second, they develop an additional adverse pressure gradient in the flow direction.

In this work, an analytical formalism has been developed to assess the implications of the presence of end reservoirs on the electroosmotic transport in narrow fluidic confinements, which may act as a convenient design basis for implementing electroosmotic flows in practical applications, without necessitating expensive computations. Toward that, usage of Schwarz–Christoffel transformation in estimating the effective electric field holds some distinct advantages. It is much faster than the computational methods, which involve mesh generation as well as time-intensive numerical computations. In the method outlined in this work, dependence of the potential field and the consequent flow solution on the geometrical parameters can readily be obtained for miniaturized fluidic devices, by convenient analytical procedures. The calibration curve presented in this study and similar other characteristic curves obtained from the analysis can contribute as potential analytical design tools for electroosmotically actuated fluidic devices, which we have verified by benchmarking with comprehensive numerical solutions.

The authors have declared no conflict of interest.

5 References

[1] Stone, H. A., Strook, A. D., Ajdari, A., *Annu. Rev. Fluid Mech.* 2004, *36*, 381–411.

[2] Conlisk, T., *Electrophoresis* 2005, *26*, 1896–1912.

[3] Kirby, B. J., Hasselbrink, E. F., Jr., *Electrophoresis* 2004, *25*, 187–202.

[4] Squires, T. M., Quake, S. R., *Rev. Modern Phys.* 2005, *77*, 977–1026.

[5] Hunter, R. J., *Zeta Potential in Colloid Science*, Academic Press, London 1981.

[6] Sun, T., Morgan, H., Green, N. G., *Phys. Rev. E* 2007, *76*, 046610 (1–18).

[7] Suh, Y. K., Heo, H. S., Park, J. H., in *Proceedings of ICNMM2006, Fourth International Conference on Nanochannels, Microchannels and Minichannels*, June 19–21, 2006, Limerick, Ireland.

[8] Zhang, Y., Gu, X. J., Barber, R. W., Emerson, D. R., *J. Colloid Interface Sci.* 2004, *275*, 670–678.

[9] Mirbozorgi, S. A., Niazmand, H., Renksizbulut, M., *J. Fluids Eng.* 2006, *128*, 1133–1143.

[10] Chakraborty, S., Padhy, S., *J. Phys. D: Appl. Phys.* 2008, *41*, 065502 (1–10).

[11] Paul, P. H., Garguilo, M. G., Rakestraw, D. J., *Anal. Chem.* 1998, *70*, 2459–2467.

[12] Dutta, D., Ramachandran, A., Leighton, D. T., Jr., *Microfluid. Nanofluid.* 2006, *2*, 275–290.

[13] Santiago, J. G., *Anal. Chem.* 2001, *73*, 2353–2365.

[14] Dutta, P., Beskok, A., *Anal. Chem.* 2001, *73*, 1979–1986.

[15] Batchelor, G. K., *An Introduction to Fluid Dynamics*, Cambridge University Press, Cambridge 1967.

[16] Milne-Thomson, L. M., *Theoretical Hydrodynamics*, McMillan & Co. Ltd, London 1962.

[17] Currie, I. G., *Fundamental Mechanics of Fluids*, McGraw-Hill Book Co., London 1974.

[18] Probstein, R. F., *Physiochemical Hydrodynamics*, Wiley, New York 1994.

[19] Patankar, S. V., *Numerical Heat Transfer and Fluid Flow*, McGraw-Hill, New York 1980.

[20] Saville, D., *Annu. Rev. Fluid Mech.* 1977, *9*, 321–337.

[21] Ghosal, S., *Annu. Rev. Fluid Mech.* 2006, *38*, 309–338.

[22] Kilic, M. S., Bazant, M. Z., Ajdari, A., *Phys. Rev. E* 2007, *75*, 021502 (1–16).

[23] Kilic, M. S., Bazant, M. Z., Ajdari, A., *Phys. Rev. E* 2007, *75*, 021503 (1–11).

[24] Abramowitz, M., Stegun, I. A. (Eds.), *Handbook of Mathematical Functions with Formulas, Graphs, and Mathematical Tables*, Dover, New York 1971.

[25] Lewin, L., *Polylogarithms and Associated functions*, North Holland, Amsterdam 1981.

[26] Roscoe, R., *Phil. Mag.* 1949, *40*, 338–351.

